

A New Model for Early Kinetic Decoupling of Dark Matter

Ivey Davis

Abstract

Dark matter has been recognized as a significant constituent of the universe. In particular, a particle species with a self annihilation cross section of $3 \times 10^{-26} \text{cm}^3 \text{s}^{-1}$, mass of $\sim 100 \text{ GeV}$ and that interacts with standard model particles via the electroweak force is of interest due to its provision of the correct dark matter abundance while also agreeing with supersymmetric expectations of a new particle species. However, it is difficult to obtain early kinetic decoupling that enhances small scale structure formation without fine tuning. In this paper, we present a new model for dark matter wherein we include an unstable standard model particle which dark matter annihilates into and can scatter off of, allowing for early kinetic decoupling without changing the properties of the particle which satisfy the "WIMP miracle".

1 Introduction

Various lines of observational evidence suggest that most of the matter in the universe is non-luminous, i.e. dark matter (DM). Despite the fact that DM makes up $\sim 80\%$ of the matter composition and roughly a quarter of the total energy density of the universe, many features of DM— including its identity— remain elusive [8]. Evidence from astronomical observations together with theoretical models of structure formation suggests that DM could consist of non-relativistic particles that have (very) weak interactions with ordinary matter, a notable example of which is weakly interacting massive particles (WIMPs) [4].

Observational constraints on DM properties arise largely from cosmic microwave background (CMB) and Lyman- α forest observations which probe the largest and smallest scales of DM respectively. The scale of temperature perturbations in the CMB as well as the way that Lyman- α forests indicate the mass quantity for a variety of redshifts help to characterize the matter power spectrum (MPS). The MPS relates density perturbations in matter to the scale of the perturbation. Perturbations of DM start to significantly grow once it dominates the energy density of the universe. However, DM particles can freely stream out of overdense regions and into underdense ones from the time they kinetically decouple from ordinary particles until the time of

matter-radiation energy density equality. The traveled distance, called the free streaming length λ_{fs} , represent the scales below which DM perturbations smooth out, which in turn affects the minimum mass of structures that can form due to gravitational collapse. The earlier the kinetic decoupling of DM particles from the early universe plasma, the smaller λ_{fs} will be [6], [5]. The moment of decoupling depends on the rate of energy transfer between the DM and ordinary particles Γ_{kin} . In general, this is related to the rate of DM annihilation into ordinary particles Γ_{ann} , which sets the DM relic abundance. Thus, lowering Γ_{kin} to have an early kinetic decoupling typically implies a smaller Γ_{ann} , and hence gives trouble in obtaining the observed DM abundance (unless there is fine-tuning). In this paper, we present a model to separate Γ_{kin} and Γ_{ann} to achieve an early kinetic decoupling without affecting the DM abundance and without fine-tuning. Specifically, we include a second, less massive particle species which the DM can maintain kinetic equilibrium through after its freeze out [10], [17]. The goal in exploring early kinetic decoupling is the boosting it provides for the production of small scale substructure. This enhancement in turn increases the likelihood of making indirect detections of DM in dwarf spheroidal galaxies through its annihilation products. The specific goal of our new model is to explore the possibility of this early kinetic decoupling without changing the relic abundance of DM.

In the following sections, we provide further background on the dynamics of DM in the early (radiation dominated) universe and the effect it has on the properties of DM today (section 1.1). This is done to provide better physical context for the differences between the model of the standard picture in section 2 and the model we introduce in section 3.1. We go into further detail on the equations we use and the results of solving them in section 3.2. We conclude the paper in section 4 with an overview of the results and significance as well as discuss considerations for future work.

1.1 Further Background

DM was initially introduced as a solution to the fact that galaxies do not exhibit rotation curves indicative of either rigid body or Keplerian motion. The role of DM in describing gravitational influences in the Universe and its effect on the development of structure was confirmed via observations of phenomena like the CMB and Lyman- α forests which give insight to the scale and distribution of density perturbations which are represented by the MPS. One of the startling qualities of DM models, particularly those which focus on “cold” DM (CDM) is just how closely they match the observed MPS spectrum. For this reason, CDM— as opposed to “warm” DM (WDM)— has been the major focus of DM investigations and searches, especially the class of DM particles known as WIMPs, which only interact with standard model particles via the electroweak force. WIMPs make a convenient candidate for DM given that its thermally averaged annihilation cross section — $3 \times 10^{-26} \text{ cm}^3\text{s}^{-1}$ — is agreed upon by both cosmological observations and supersymmetric particle physics models for a mass of 100 GeV in such a serendipitous way as to be dubbed the “WIMP miracle”.

CDM gets its name following its definition of being nonrelativistic. The importance

of its nonrelativistic quality is manifested in its free streaming length. The effect that a particle’s velocity has on its free streaming length can be thought of in the context of considering density perturbations as gravitational wells; the greater the perturbation, the higher the particle’s velocity needs to be in order to escape the perturbation. Therefore, CDM is confined to smaller density perturbations, which is equivalent to saying that its λ_{fs} is small. This is in contrast to the more relativistic WDM whose velocities are such that they can escape the small scale perturbations and hence smooth them out. In this way, CDM promotes small scale structure formation while WDM promotes structure formation on the large scale. This further means that CDM promotes a “bottom up” evolution for galaxy formation, wherein the favored small scale substructures eventually amalgamate into the larger galactic and galactic cluster scales that we observe today.

The velocity of DM is set by its temperature at the time of its kinetic decoupling. When the particles are nonrelativistic but still coupled to the thermal bath, then the kinetic energy of the particle is given by the expression of a fluid in thermal equilibrium: $3k_B T = mv^2$ so that $v \propto \sqrt{T}$. At the point of kinetic decoupling, the DM particle ceases to interact with the primordial plasma and leaves thermal equilibrium such that $v \propto T$. The temperature scales inversely with the scale factor of the universe a – i.e. the temperature of the universe drops as it increases in size – so that $v \propto a^{-1}$ post-decoupling. The scale of the largest perturbation is restricted by the scale factor, hence earlier decoupling and larger T implies a smaller a and smaller free streaming length. More explicitly:

$$\lambda_{fs} = \int_0^{t_{eq}} \frac{v(t)}{a(t)} dt \approx r(t_{NR}) \left(1 + \frac{1}{2} \log \frac{t_{eq}}{t_{NR}}\right) \quad (1)$$

where t_{NR} is the time when the DM becomes nonrelativistic, t_{eq} is when the DM leaves kinetic equilibrium, and $r(t_{NR})$ is the comoving size of the horizon at t_{NR} [18]. The importance in favoring a small streaming length and enhancing the small scale substructure is that the chances of making indirect detections of DM via annihilations are increased due to an increased density of substructure [16]. Therefore, in the next sections, we will discuss the physics of the standard picture to emphasize why the introduction of a new model is important in increasing the likelihood of indirect detections of DM.

2 The Standard Picture

In the standard picture, the DM particle χ can annihilate into much smaller particles ϕ such that $\chi\chi \leftrightarrow \phi\phi$ and can scatter off of ϕ particles like $\chi\phi \leftrightarrow \chi\phi$. The rate of energy transfer Γ_{kin} is proportional to the product of the thermally averaged scattering cross section $\langle \sigma_{sc} v \rangle$ and the equilibrium number density of ϕ – the number density of ϕ that allows thermal equilibrium with the ambient plasma – n_ϕ^{eq} that is given as a function of temperature T in equation 2, where p is the momentum for the particle

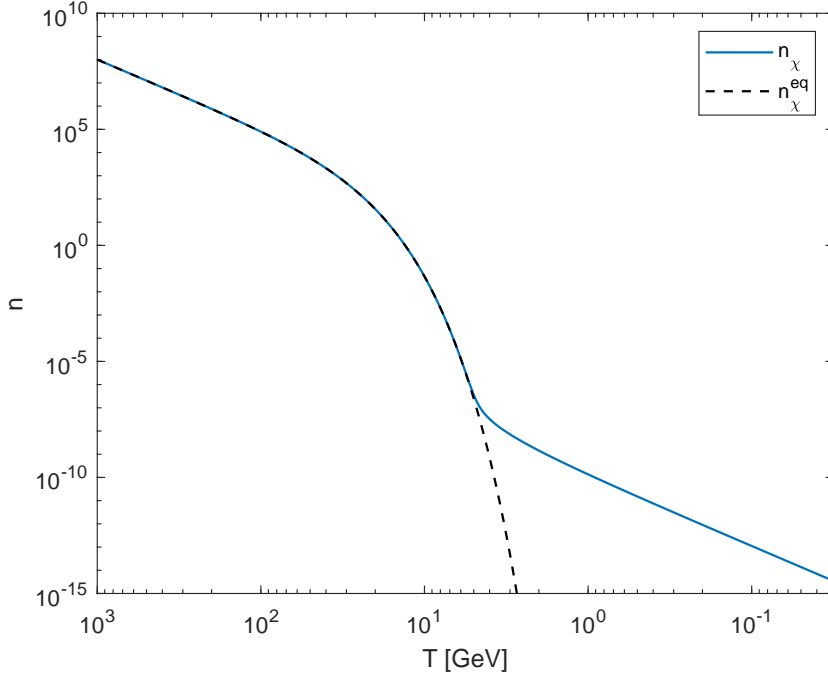


Figure 1: The solution for equation 6 as well as the equilibrium number density given in equation 2. As this shows, n_χ tracks n_χ^{eq} for $T > m_\chi$ when both the annihilation and inverse processes can occur. When T drops below the mass (100 GeV), the inverse process can no longer be supported and the number density decreases rapidly. This accelerated decrease in n_χ continues until $T \sim m/22$, at which point Γ_{ann} drops below H and n_χ freezes out.

and m is the mass. Similarly, the annihilation rate of χ is proportional to the product of the thermally averaged *annihilation* cross section $\langle \sigma_{ann} v \rangle$ and the χ equilibrium number density n_χ^{eq} .

$$n_{eq} = \frac{4\pi}{(2\pi)^3} \int_0^\infty p^2 e^{\sqrt{p^2+m^2}/T^2} dp \quad (2)$$

The interaction between χ and ϕ is described by the Boltzmann equation in equation 3 [13], [14]. On the left hand side, $\mathbf{L}[f]$ is the Liouville operator that describes the time evolution of the phase space density and $\mathbf{C}[f]$ is the collision operator which describes the type of interactions that can occur between χ and ϕ .

$$\mathbf{L}[f] = \mathbf{C}[f] \Rightarrow \frac{dn_\chi}{dt} = -3Hn_\chi - \langle \sigma_{ann} v \rangle (n_\chi^2 - n_{eq}^2) \quad (3)$$

On the right hand side, the expansion rate of the universe H during the radiation dominated era as function of time is given as:

$$H = \frac{1}{2t} \quad (4)$$

Using natural units, where $\hbar = c = k_b = 1$, mass and temperature can both be expressed in units of energy. With this convention, the point where the temperature $T \lesssim m_\chi$, where m_χ is the mass of the χ particle, the $\chi\chi \leftrightarrow \phi\phi$ expression is no longer two way as the ambient temperature of the thermal bath is no longer sufficient to support the inverse annihilation process of the ϕ particles back into χ . This causes n_χ to begin dropping rapidly and χ becomes nonrelativistic. Further, the dependence of Γ_{ann} on n_χ causes the annihilation rate to drop below H for sufficiently low T ; the expansion rate of the Universe becomes greater than the interaction rate between χ particles, hence preventing them from further annihilating with each other. Because they can no longer annihilate, the number of χ particles remains constant with comoving volume and is considered to be frozen out; the relic number density is set. This happens at a temperature $T_{fr} \sim m_\chi/20$, or about 5 GeV for a 110 GeV particle like we consider [14].

Although, the χ particles have stopped annihilating, they can still scatter off of the ϕ particles and maintain kinetic equilibrium until $\Gamma_{kin} < H$. However, because $\langle \sigma_{sc}v \rangle \approx \langle \sigma_{ann}v \rangle$, the difference between Γ_{ann} and Γ_{kin} is dependent on the difference between the number densities of the ϕ and χ particles. Because the ϕ particle is so light – essentially massless compared to the χ particle– the n_ϕ does not freeze out until much later and hence $\Gamma_{kin} \gg \Gamma_{ann}$. Therefore, the kinetic decoupling occurs much later than freeze out, at a temperature $T_{kd} \sim 1$ MeV [7]– roughly the temperature of neutron freeze out [15]– as compared to the ~ 1 GeV freeze out temperature for a canonical WIMP mass. To get earlier decoupling in this model, there typically needs to be significant fine tuning regarding the cross section of the DM [11], which then affects the DM relic abundance. The goal of the model presented next is to push T_{kd} closer to T_{fr} without this fine tuning so that the correct relic abundance can be preserved.

3 The New Model

3.1 Theory

In the model we use for this work, we consider a similar interactive circumstance as in the standard picture where χ can annihilate into and scatter off of a lighter particle species. However, the annihilation product considered here, χ' , is much more massive than the ϕ particle with $m_\chi \gtrsim m_{\chi'}$. The χ' is also unstable and thus decays like $\chi' \rightarrow \psi\psi$ at some rate Γ_{dec} where $m_\chi, m_{\chi'} \gg m_\psi$. Although there are now three particle species to consider, because χ' is so massive, interactions between χ and ψ particles are negligible; processes like $\chi\chi \leftrightarrow \psi\psi$ and $\chi\psi \leftrightarrow \chi\psi$ are suppressed. Again, once $\Gamma_{ann} < H$ (still at $T \sim m_\chi/20$), the χ particle's number density freezes out, setting the relic number density. However, the decaying property of χ' means its number density isn't strictly dependent on n_χ and hence Γ_{kin} and Γ_{ann} are no longer so heavily linked. Because the χ' particle is so massive and is also experiencing decay, its freeze out can happen much earlier than in the case of the ϕ particle and kinetic decoupling can occur much closer to the freeze out of χ . This is all to say that the

$\chi\chi \leftrightarrow \chi'\chi'$ process sets the relic abundance while the $\chi\chi' \leftrightarrow \chi\chi'$ process governs the kinetic decoupling, thereby making early kinetic decoupling possible without altering the cross section– and hence the relic abundance– of DM.

3.2 Methods and Results

In order to understand how the temperature of the χ particle evolves with the temperature of the ambient plasma, it's convenient to express the Boltzmann equation from equation 3 in terms of temperature using the following expression for time:

$$t = \frac{1}{4} \sqrt{\frac{90}{\pi^2 g}} \frac{m_p}{T^2} \quad (5)$$

where m_{pl} is the Planck mass and g is the number of relativistic degrees of freedom. This then gives the temperature derivative of n_χ as:

$$\frac{dn_\chi}{dT} = \sqrt{\frac{90}{\pi^2 g}} \frac{m_p}{T^3} [3Hn_\chi + \langle \sigma_{ann} v \rangle (n_\chi^2 - n_{\chi,eq}^2)] \quad (6)$$

Because of the role that χ' plays in kinetic decoupling, we also include an equation which accounts for the evolution of the $n_{\chi'}$ particle, given as:

$$\frac{dn_{\chi'}}{dT} = \sqrt{\frac{90}{\pi^2 g}} \frac{m_p}{T^3} [3Hn_{\chi'} + \langle \sigma_{ann} v \rangle (n_{\chi'}^2 - n_\chi^2) + \Gamma_{dec}(n_{\chi'} - n_{\chi',eq})] \quad (7)$$

There are a couple of distinctions between equations 6 and 7. The most obvious difference is the inclusion of the $\Gamma_{dec}(n_{\chi'} - n_{\chi',eq})$ term in equation 7 which accounts for the decay of χ' . The second, perhaps more subtle difference, is the $\langle \sigma_{ann} v \rangle (n_{\chi'}^2 - n_\chi^2)$ term. The inclusion of n_χ is what couples equation 7 to equation 6; although n_χ evolves independently of the properties of χ' that we consider here, the role of χ in the production of χ' means n_χ must be included here to obtain the correct $n_{\chi'}$.

The numerical solutions of $n_{\chi'}$ from these coupled equations, found using MATLAB's ODE15s solver (see appendix A for a more detailed discussion of the programming methods) are shown in figure 2 when using $g = 100$, the canonical annihilation and scattering cross sections of $3 \times 10^{-26} \text{ cm}^3\text{s}^{-1} \approx 2.5 \times 10^{-9} \text{ GeV}^{-2}$, a mass $m_\chi = 110 \text{ GeV}$ that is consistent with such a cross section, and a decay rate of 10^{-5} GeV . As expected, χ freezes out at $T \approx 5 \text{ GeV}$ regardless of the mass of χ' , and the smaller $m_{\chi'}$ the later the freeze out of $n_{\chi'}$. An important feature of this plot is that even for $m_\chi = m_{\chi'}$, $n_{\chi'}$ still freezes out later than n_χ ; freeze out of $n_{\chi'}$ cannot occur until after χ particles stop annihilating and producing χ' particles. Also as expected, the case of $m_{\chi'} = 0$, which is representative of the standard picture, shows the freeze out of χ' happening for much lower temperatures, hinting at the late kinetic decoupling predicted by the standard picture.

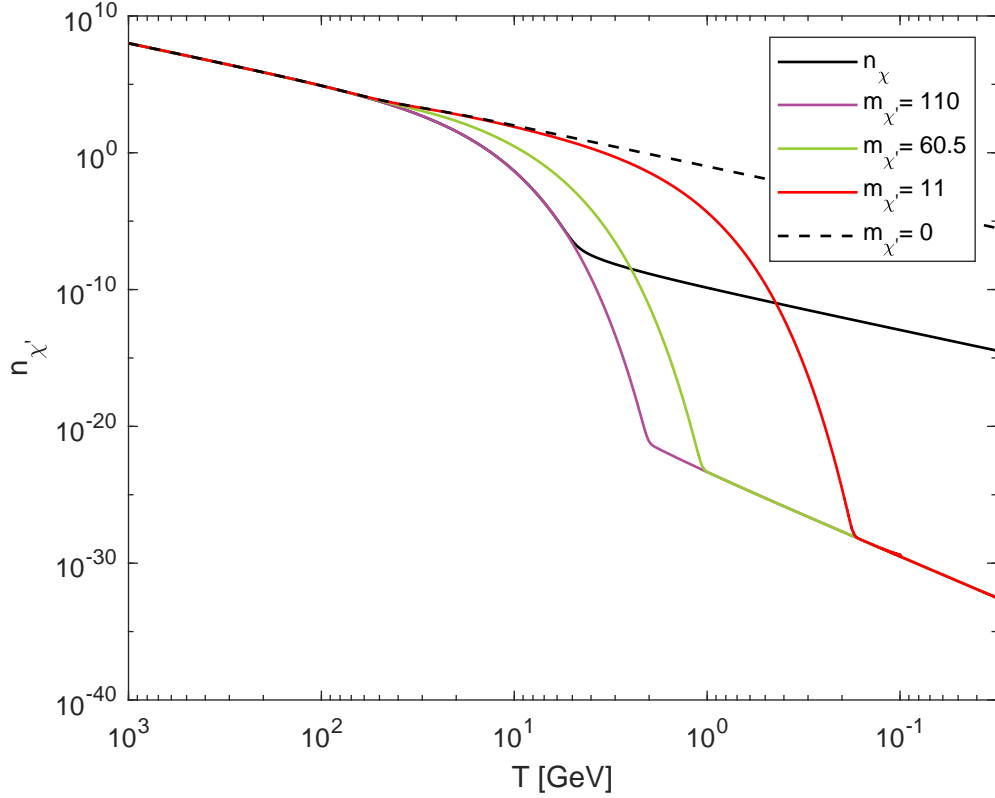


Figure 2: The solutions for $n_{\chi'}$ for various $m_{\chi'}$. The solution for n_{χ} – which is independent of the mass of χ' – is also included here in order to give a better sense of the difference in scales of n_{χ} and $n_{\chi'}$ at the times of their freeze out. $m_{\chi'} = 0$ is representative of the standard picture case. As this shows, the more massive χ' is, the closer its freeze out occurs to the freeze out of χ .

To find when kinetic decoupling occurs, we then introduce the following equation which describes how the temperature of χ , T_χ , evolves with the ambient temperature (for example see [19]):

$$\frac{dT_\chi}{dT} = -\sqrt{\frac{90}{\pi^2 g}}(\alpha \langle \sigma_{ann} v \rangle n_{\chi'}(T - T_\chi) - 2HT_\chi) \quad (8)$$

Here, α is a kinematic factor that accounts for the amount of energy transferred per scattering; $\alpha \sim T/m_\chi$ for $T > m_{\chi'}$ and $m_{\chi'}/m_\chi$ for $T < m_{\chi'}$. This expression is coupled to equations 6 and 7 through its dependence on $n_{\chi'}$.

The solution for this is shown in figure 3. While the χ particle is still kinetically coupled to the thermal bath, its temperature is the same as the ambient temperature, just as it should be. Then the point where T_χ goes from being proportional to T and begins being proportional to T^2 is when kinetic decoupling occurs. For $m_{\chi'} = m_\chi$, this happens at $T_{kd} \approx 4.5$ GeV, a temperature three orders of magnitude higher than is provided by the standard picture.

The significant difference in the kinetic decoupling temperatures is made even more apparent when considering the effect it has on the scale of the free streaming mass M_{fs} . We use the following expression:

$$M_{fs} \approx 2.9 \times 10^{-6} \left[\frac{1 + \ln(g^{1/4} T_{kd}/50)/19.1}{(m_\chi/100)^{1/2} g^{1/4} (T_{kd}/50)^{1/2}} \right]^3 M_\odot \quad (9)$$

where T_{kd} is in MeV and m_χ is in GeV. Plugging the appropriate values into this equation then gives an M_{fs} of $2.026 \times 10^{-10} M_\odot$. This is ~ 5 orders of magnitudes smaller than the $1.76 \times 10^{-5} M_\odot$ that's achieved in the case of the standard picture. Therefore, replacing the massless particle of the standard picture with an unstable, massive particle allows us to drastically decrease the lower limit on the mass of the substructure which the DM can produce, suggesting we should be much more likely to witness the products of annihilation events and hence indirectly detect DM.

4 Conclusion

Despite the significant contribution that DM makes to the mass and total energy densities of the Universe, the actual identity of DM still eludes us ([3], [9], and [12] provide good reviews). What we do know about DM is highly influenced by the MPS. What it suggests is that DM was nonrelativistic when it kinetically decoupled from the thermal bath of the early Universe in order to support the presence of small scale structures in a bottom-up approach to the construction of large scale structures. Assuming a thermal production method for DM, then we also find an annihilation cross section that coincidentally agrees with supersymmetric expectations for the annihilation cross section of a 100 GeV particle that interacts with standard model particles via the electroweak force. This inclines us to favor such particles in models.

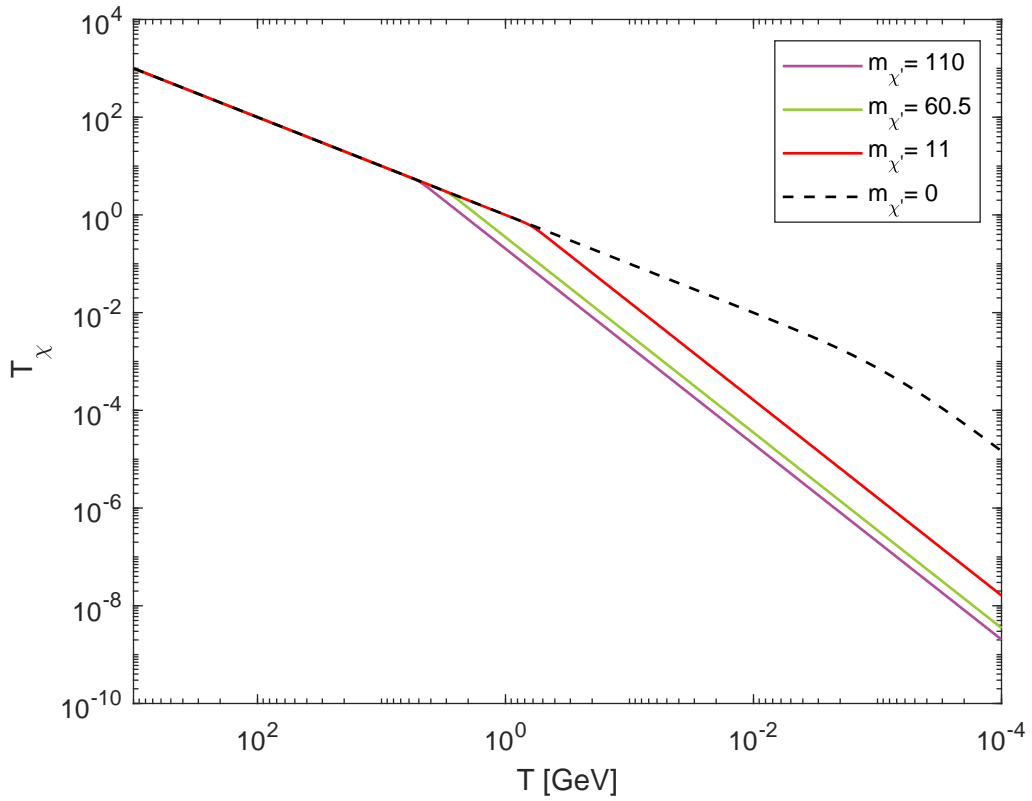


Figure 3: The solution of T_χ following the simultaneous solving of equations 6, 7, and 8. $m_{\chi'} = 0$ is representative of the standard picture case, and shows kinetic decoupling occurring at $T_{kd} \sim 1\text{MeV}$.

All of these properties provide important restrictions for modelling DM. However, in the standard picture where DM interacts with an essentially massless particle species, it is difficult to get early kinetic decoupling– and hence small free streaming lengths– without fine tuning the annihilation cross section. In order to get early kinetic decoupling without fine tuning, we use a massive, unstable particle in place of the massless one. By doing this, we find DM kinetically decoupling at a temperature three orders of magnitude higher than in the standard picture case, which corresponds to a free streaming mass scale five orders of magnitude smaller than the standard picture predicts without changing the relic abundance.

In pushing down the lower limit of the free streaming mass, the protohalo substructure density is significantly enhanced. Because we didn't need to decrease the annihilation cross section or rate to get the earlier decoupling, this then suggests that in this model we are more likely to indirectly observe DM through the products of annihilation events. Furthermore, the 110 GeV DM mass that we use is ideal for direct detection searches that use a scattering target like Xenon with a nuclear mass of 120 GeV [1], [2] while still being consistent with WIMP mass expectations.

The particle physics of the massive annihilation product of DM is a point of interest for future work. It is also important to consider this model in the context of nonstandard thermal histories, namely when an early matter domination era is considered. In this case, matter domination occurs before big bang nucleosynthesis, which has an interesting impact on the evolution of the scale factor, the expansion rate of the Universe, and consequently when freeze out and kinetic decoupling can occur and when structures can begin forming [19]. This is therefore a topic of major interest for future work.

Acknowledgements

I would like to thank my research advisor Dr. Rouzbeh Allahverdi for his encouragement and guidance throughout this project. I would also like to thank Dr. Jaksa Osinski for his support, especially in reviewing and providing suggestions for the code for this project. Many thanks are also due to Mr. Charles Rayburn of the Rayburn Reaching Up Fund and the National Science Foundation (grant number PHY-1720174) for financially supporting this work.

References

- [1] D.S. Akerib, H.M. Araújo, X. Bai, A.J. Bailey, J. Balajthy, P. Beltrame, E.P. Bernard, A. Bernstein, T.P. Biesiadzinski, E.M. Boulton, and et al. Improved limits on scattering of weakly interacting massive particles from reanalysis of 2013 lux data. *Physical Review Letters*, 116(16), Apr 2016.

- [2] E. Aprile, M. Alfonsi, K. Arisaka, F. Arneodo, C. Balan, L. Baudis, B. Bauermeister, A. Behrens, P. Beltrame, K. Bokeloh, and et al. Dark matter results from 225 live days of xenon100 data. *Physical Review Letters*, 109(18), Nov 2012.
- [3] Howard Baer, Ki-Young Choi, Jihn E. Kim, and Leszek Roszkowski. Dark matter production in the early universe: Beyond the thermal wimp paradigm. *Physics Reports*, 555:1–60, Feb 2015.
- [4] Gianfranco Bertone, Dan Hooper, and Joseph Silk. Particle dark matter: evidence, candidates and constraints. *Physics Reports*, 405(5-6):279–390, Jan 2005.
- [5] Torsten Bringmann. Particle models and the small-scale structure of dark matter. 2009.
- [6] Torsten Bringmann and Stefan Hofmann. Thermal decoupling of wimps from first principles. 2006.
- [7] Xuelei Chen, Marc Kamionkowski, and Xinmin Zhang. Kinetic decoupling of neutralino dark matter. *Physical Review D*, 64(2), Jun 2001.
- [8] Planck Collaboration. Planck 2018 results. vi. cosmological parameters, 2018.
- [9] P. S. Bhupal Dev, Anupam Mazumdar, and Saleh Qutub. Constraining non-thermal and thermal properties of dark matter. *Frontiers in Physics*, 2:26, 2014.
- [10] Jeff A. Dror, Eric Kuflik, Brandon Melcher, and Scott Watson. Concentrated dark matter: Enhanced small-scale structure from codecaying dark matter. *Phys. Rev. D*, 97:063524, Mar 2018.
- [11] Adrienne L. Erickcek, Kuver Sinha, and Scott Watson. Bringing isolated dark matter out of isolation: Late-time reheating and indirect detection. *Physical Review D*, 94(6), Sep 2016.
- [12] Gian Francesco Giudice, Edward W. Kolb, and Antonio Riotto. Largest temperature of the radiation era and its cosmological implications. *Physical Review D*, 64(2), Jun 2001.
- [13] Edward W. Kolb and Michael S. Turner. *The early universe*, volume 69. 1990.
- [14] Edward W. Kolb and Stephen Wolfram. Baryon number generation in the early universe. 1980.
- [15] Mariangela Lisanti. Lectures on dark matter physics. *New Frontiers in Fields and Strings*, Nov 2016.

- [16] Kenny C.Y. Ng, Ranjan Laha, Sheldon Campbell, Shunsaku Horiuchi, Basudeb Dasgupta, Kohta Murase, and John F. Beacom. Resolving small-scale dark matter structures using multisource indirect detection. *Physical Review D*, 89(8), Apr 2014.
- [17] Shohei Okawa, Masaharu Tanabashi, and Masato Yamanaka. Relic abundance in a secluded dark matter scenario with a massive mediator. 2017.
- [18] A. Schneider, R. E. Smith, and D. Reed. Halo mass function and the free streaming scale. *Monthly Notices of the Royal Astronomical Society*, 433(2):1573–1587, Jun 2013.
- [19] Isaac Raj Waldstein, Adrienne L. Erickcek, and Cosmin Ilie. Quasidecoupled state for dark matter in nonstandard thermal histories. *Physical Review D*, 95(12), Jun 2017.

A Programming Methods

The evaluations of the differential equations presented in this paper were done using MATLAB's ODE15s solver. These expressions cannot be solved analytically and we further experienced two main issues when trying to solve the expressions numerically. The first was the solver's ability to accommodate the stiffness of the expression, especially where the number density is Boltzmann suppressed and drops several orders of magnitude rapidly. The second issue was the machine's ability to accommodate the precision necessary for numerical analysis of the small number densities post-freeze out.

These problems are initially solved by splitting up the original thermal bath temperature range of interest T_{rang} into a collection of smaller temperature intervals T_{int} . ODE15s is then run on each of these intervals and uses the final solution of an interval as the initial values for the following interval, where the very first initial condition is that the number densities are at the equilibrium value, which is valid for $T \gg m_\chi$. This works well especially for the first problem described, however, additional issues arise in regards to the second problem. Specifically, not many intervals are necessary for the evaluation at higher temperatures, but many are needed to get the appropriate precision of the small number densities at lower temperatures. Given that T_{rang} spans ~ 6 orders of magnitude and that T_{int} needs to be roughly on the order of 10^{-3} to get solutions for $T \lesssim 1$, a static T_{int} would require 10^9 iterations to evaluate the entire temperature range. This just wasn't feasible considering the hardware available (my personal laptop).

In order to reach the necessary precision in the solution without increasing the number of intervals to unreasonably high numbers, we employ a dynamic step size that is dependent on the order of magnitude of the most recently used thermal bath temperature. At each iteration, the step size is set to two orders of magnitude less than the last value of the temperature that was used, *e.g.* if the temperature is 500 GeV, the step size is 1 GeV. This reduces the number of intervals necessary to evaluate the same 6 orders of magnitude to less than 10,000. Figure 4 shows what the solutions look like if MATLAB tries to solve the entire 1000 GeV temperature range at once. A comparison between the solutions provided by equal sized steps and by dynamic step sizes are shown in figures 5 and 6. It's obvious from these figures that using a dynamic step size significantly improved not only the solutions, but also the processing time necessary to achieve them.

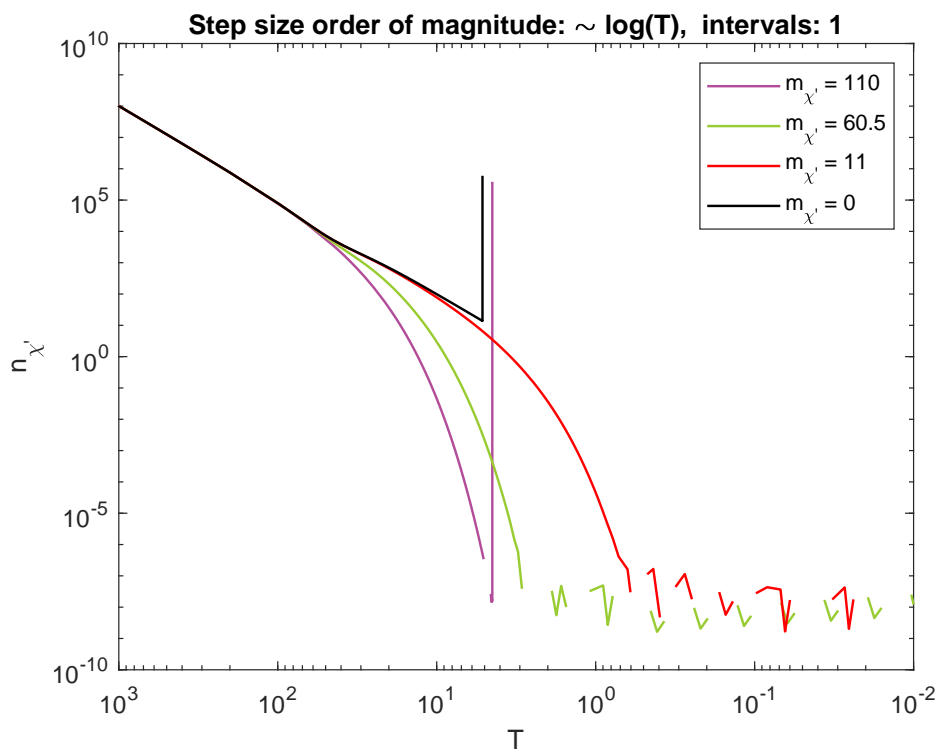
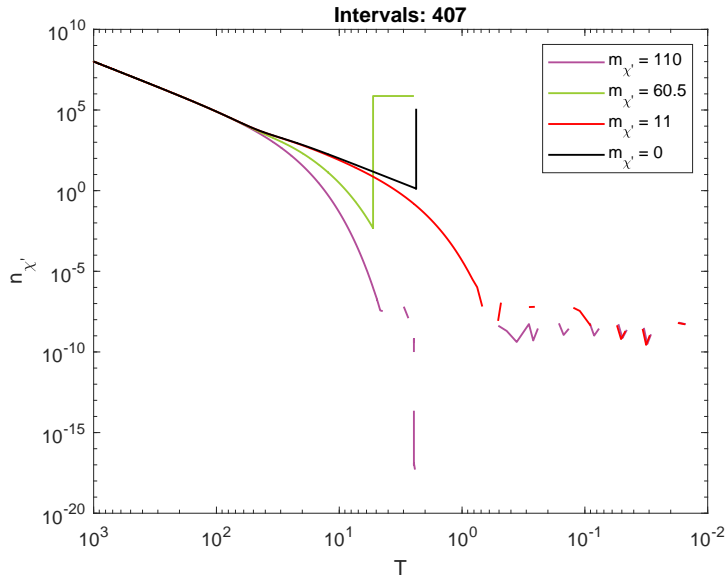
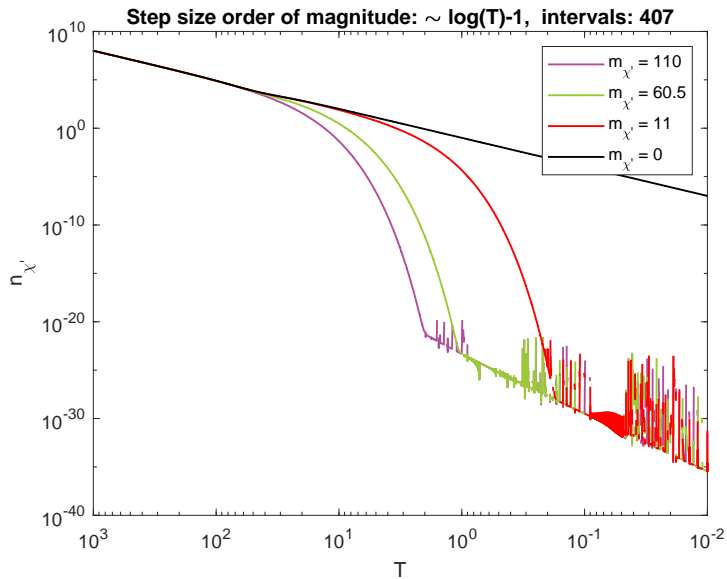


Figure 4: The solutions of equations 6 and 7 when ODE15s is given the entire temperature range at once .

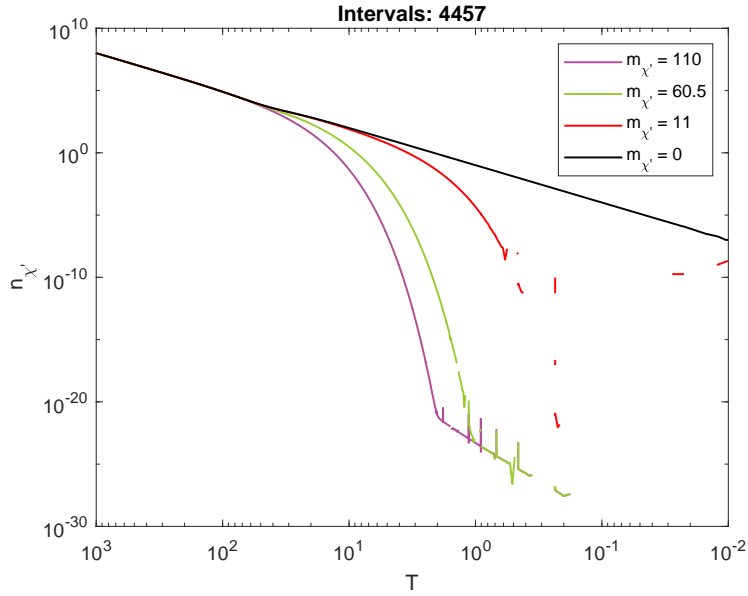


(a) The solution to equation 7 if the evaluation interval size is fixed (~ 2.5 GeV per iteration).

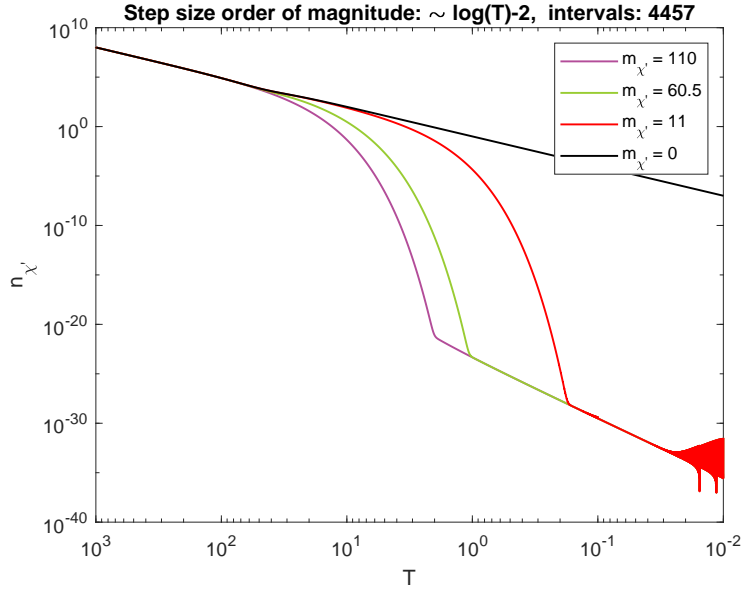


(b) The solution to equation 7 if the evaluation interval size is one order of magnitude smaller than the temperature being evaluated (*i.e.* when $T = 500$ GeV, $T_{int} = 10$ GeV).

Figure 5: A comparison of the solution for equation 7 if a dynamic step size is used as opposed to a static one. For the same number of intervals, the solutions from using a dynamic step size are significantly better.



(a) The solution to equation 7 if the evaluation interval size is fixed (~ 0.22 GeV per iteration).



(b) The solution to equation 7 if the evaluation interval size is two orders of magnitude smaller than the temperature being evaluated (*i.e.* when $T = 500$ GeV, $T_{int} = 1$ GeV).

Figure 6: A comparison of the solution for equation 7 if a dynamic step size is used as opposed to a static one, with the number of steps being $\sim 10\times$ greater than used in figure 5.